DD

ISSN 1346-244X
RIKEN-AF-NP-383

Time and Energy Responses of Liquid-Xenon Scintillation Chamber for ^{20}Ne Ion Beam at 135*A* MeV

T. Kato, T. Doke, J. Kikuchi, F. Nishikido, H. Okada, K. Morimoto, and I. Tanihata

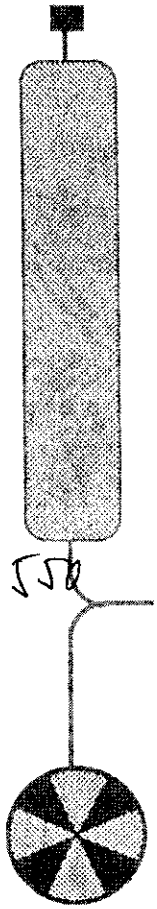

RIKEN
ACCELERATOR
RESEARCH
FACILITY

March 2001

The Institute of Physical and Chemical Research (RIKEN)
2-1 Hirosawa, Wako, Saitama 351-0198, Japan
TEL: (048)462-1111 FAX: (048)462-4642
e-mail: *username*@rikvax.riken.go.jp

Typeset using jjap.cls <ver.1.0.1>

Time and Energy Responses of Liquid-Xenon Scintillation Chamber for ^{20}Ne Ion Beam at 135A MeV

Toshiyuki KATO*[1], Tadayoshi DOKE, Jun KIKUCHI, Fumihiko NISHIKIDO, Hiroyuki OKADA, Kouji MORIMOTO*[2] and Isao TANIHATA*[2]

Kikuicho-Branch, Advanced Research Institute for Science and Engineering, Waseda University, 17 Kikuicho, Shinjuku-ku, Tokyo 162-0044, Japan

(Received)

The time and energy responses of a liquid-xenon (LXe) scintillation chamber to heavy-ion beams were studied using ^{20}Ne ions at an energy of 135A MeV. The scintillation light in LXe was observed by two photomultipliers (PMTs). The intrinsic time resolution by one PMT was confirmed to be approximately 30 ps in sigma up to a beam intensity of 1.3×10^5 counts per second (cps). The energy output was observed to be also constant for the increase in the beam intensity. The energy resolution was 1.2-1.4 % in sigma. The possibilities of LXe as a detector medium for an energy spectrometer and a timing detector for heavy-ion beams were described.

KEYWORDS: liquid xenon, scintillation chamber, heavy ion, energy resolution, time resolution, beam intensity, RI beam

*[1] E-mail address: tkato@riken.go.jp

*[2] Present address: The Institute of Physical and Chemical Research (RIKEN), 2-1 Hirosawa, Wako, Saitama 351-0198, Japan.

1. Introduction

In the RI Beam Factory project at the Institute of Physical and Chemical Research (RIKEN), various RI's are produced by projectile fragmentation. Discoveries of numerous new isotopes heavier than O are expected.[1,2] A high-momentum fragment is separated and identified by use a combination of a magnetic field analyzer, a time-of-flight (TOF) mass spectrometer, an energy loss counter and a total-energy calorimeter.

Conventionally, Si detectors have been used for precise energy loss or total-energy measurement because they have excellent energy resolution for charged particles. However, they are very weak against radiation damage by heavy charged particles. Namely, Si detectors have good energy resolution because of their small band gap due to its crystal structure but the regular structure is easily broken along the track of incident heavy particles. The result produces irreversible radiation damage. In a long-term experiment, accordingly, we have to pay attention to the amount of beam irradiation and sometimes replace the Si detectors during the experiment. To search for new isotopes in a region away from the stability line in the nuclear chart, the amount of beam irradiation required will be more because of the low production cross sections of these nuclei. Therefore, the detectors, which are resistant to radiation damage due to heavy particles, are required.

To satisfy such a requirement, the possibility of the use of liquid rare gas as a detector medium was considered for detectors which are resistant to irradiation damage by heavy particles. Recently, a new liquid argon (LAr) ionization chamber had been constructed and tested for heavy ions of approximately 100A MeV[3,4] energy. Excellent energy resolutions of $0.6 - 0.7\%$ in full width at half maximum (FWHM) were achieved for Ar and Ca beams.[3] but the pulse heights of ionization signals from the chamber changed with the beam intensity as a result of the accumulation of Ar^+ ions.[4]

To eliminate such an intensity dependence of output pulse heights, in the next step, the use of scintillation light from liquid xenon (LXe) was considered. The wavelength of the scintillation light is ultraviolet (around 175 nm[5]) but still sufficient long to be measured by a photomultiplier (PMT) directly. In addition, the decay time constants (4.3 and 22 ns) [6] are comparable to those of plastic scintillators, and the scintillation

yield ($W_{ph} = 14.7$ eV[7]) is also comparable to that in a NaI(Tl) crystal.

Based on the above-mentioned considerations, we have recently constructed a LXe scintillation chamber for heavy charged particles and tested it with ^{20}Ne ions at an energy of 135.4 MeV from the RIKEN Ring Cyclotron (RRC) for stability with beam intensity, time resolution and energy resolution. In this paper, the results of the experiment will be reported and a new chamber for real nuclear physics experiments designed based on newly obtained data will be presented.

2. LXe scintillation chamber

2.1 Chamber

The LAr ionization chamber used in the experiment[3,4] has been improved for the present scintillation experiment. Figure 1 shows a cross-sectional view of the LXe scintillation chamber. It consists of an internal vessel and a cryostat system. The internal vessel is placed in vacuum, and wrapped by superinsulators, which prevent heat flow due to radiation to the vessel. The internal vessel was kept at a LXe temperature of -110 °C by the cryostat filled with a mixture of ethanol and liquid N_2 as shown in the figure.

The heavy-ion beam comes into the internal vessel through an aluminized Mylar foil of 100 μm thickness and a Havar foil of 160 μm thickness. Figure 2 shows cross-sectional views of the internal vessel as well as PMTs, which are attached to the outer vessel. The Havar foil is welded on a stainless-steel flange and supported by a stainless-steel fin-type lattice. The width of the fin-type lattice is 2 mm and the pitch is 10 mm. The thickness of the fin-type lattice is 10 mm and sufficient to stop the ^{20}Ne beam of 135.4 MeV.

Liquid xenon (400 ml) fills the vessel. Its volume is defined by a cylindrical black Alumite, which has zigzag surface to reduce reflection of scintillation light.[8] The internal vessel of the LXe scintillation chamber and the lines of the purification and liquefaction system were baked and vacuumed at 120 °C and 150 °C, respectively, for several days to maintain the cleanliness of the system. Xenon gas was purified with Ba-Ti getters, and then condensed into the internal vessel. The LXe purity of less than 100 ppb as oxygen equivalent impurity concentration was achieved.

Liquid xenon must be kept at a zero electric field in the metal wall because the scintilla-

tion efficiency of LXe depends on an electric field significantly. A grounded shielding grid, which has 96% open space, eliminates the electric field from the PMTs. The transparency of a 5-mm-thick MgF_2 window to VUV light from Xe atoms is about 90% nominally. It is sealed in a stainless-steel flange by indium packing.

2.2 Photomultipliers for the LXe scintillation chamber

Scintillation light is observed by two PMTs (PMT A and PMT B) through the MgF_2 window of the internal vessel and the quartz windows of PMTs, 2 mm in thickness. The dimensions of the PMT (Hamamatsu R5900) are $27\times27\times22$ mm^3 and the effective area of the photocathode is 18×18 mm^2, which is composed of Rb, Cs and Sb. The nominal quantum efficiency to 175 nm VUV light is about 10%. It has a metal-channel dynode and has 10 stages. The high-voltage divider for the LXe scintillation chamber is shown in Fig. 3. In order to remove an unstable response to fluctuation of a beam intensity due to the lack of the divider current, the total divider resistance was reduced from 36 MΩ to 720 kΩ. The divider current of 1.4 mA at an applied voltage of 1 kV also stabilizes the PMT response for a large amount of light produced by irradiation of heavy-ion beams. The boosters (HV1-3) allow the PMT to work stably under a high-intensity beam. The signal were detected from the anode, the 9_{th} dynode(Dy1) and the 8_{th} dynode(Dy2). Dy1 and Dy2 were used in this experiment for the ^{20}Ne beam because the gain with all stages of the dynode was too high to precisely observe the light produced without a sign of saturation of an anode signal.

3. Experiment with ^{20}Ne beam

3.1 Experimental setup

Figure 4 shows the experimental arrangement. The ^{20}Ne beam was extracted through a Mylar window of 300 μm thickness. Two PMTs (Hamamatsu H1161) were attached on either side (the left (L) and the right (R) sides) of a 1-mm-thick plastic scintillator (BICRON 408). This scintillation counter was used as one of the triggers and as the start of TOF. The distance between the plastic scintillator and the internal vessel of the LXe scintillation chamber defined the flight length to be 80 cm. The veto counter consisted of a plastic scintillator of 1 mm thickness with a 1-mm-diameter hole at the center of the

effective area, which was used to define the beam position within the hole. It was aligned to the beam axis and the center of the LXe scintillation chamber. All ^{20}Ne ions stopped in LXe, and their scintillation light was measured by two PMTs.

3.2 Experiment

The performance of the LXe scintillation chamber was investigated with an ^{20}Ne beam of 135*A* MeV energy at a beam intensity up to 1.3×10^5 cps. The energy resolution, the time resolution and the response to the beam intensity were studied. Aluminum plates of 0, 1, 3, 5, 8 and 10 mm thicknesses were placed before the plastic scintillator as a degrader to change the beam energy.

4. Results and discussion

4.1 Time resolution

Signals of Dy2 from both PMTs were discriminated by a discriminator (Phillips 730) in the leading edge, and then connected to the stop of TDC (Kaizu 3780). The bin width of the TDC was 25 ps. The coincidence signal of the plastic scintillator and the LXe scintillation chamber was used as a start of the TDC. A fluctuation of the start signals is completely eliminated by reconstructing a spectrum of the time difference between two channels of the TDC.

Figure 5 shows a typical time-difference spectrum to the ^{20}Ne ion beam between PMT A and PMT B. A time walk effect, which was caused by the discrimination in the leading edge at various pulse heights, was corrected in the time-difference spectrum. The correction, however, did not give much influence on the time resolution because of the good uniformity of the pulse heights. The width of the spectrum ($\sigma(A-B)$) is written as follows,

$$\sigma(A-B)^2 = \sigma(A)^2 + \sigma(B)^2, \tag{4.1}$$

where $\sigma(A)$ and $\sigma(B)$ are the time resolutions of PMT A and PMT B, respectively. $\sigma(A-B)$ was 41 ps. Assuming that $\sigma(A)$ and $\sigma(B)$ were the same, the intrinsic time resolution of 29 ps is obtained by dividing $\sigma(A-B)$ by $\sqrt{2}$.

Figure 6 shows the intensity dependence of the intrinsic time resolution in the LXe scintillation chamber. As observed from the figure, it was constant at approximately

30 ps in sigma up to a beam intensity of 1.3×10^5 cps. The vertical error bars include fluctuations due to the bining and the statistical error, and the horizontal ones were given for the minimum and maximum beam intensities in each measurement.

Since the mean of values obtained from two PMTs is used for the TOF measurement, the time resolution of the LXe scintillation chamber with two PMTs is given by dividing the intrinsic time resolution of 30 ps by $\sqrt{2}$. It is 21 ps in sigma.

4.2 Energy output and resolution

Typical energy spectra of Dy1 and Dy2 for the ^{20}Ne ion beam are shown in Figs. 7(a) and 7(b). They were reconstructed by summing both ADCs of PMT A and PMT B. The energy resolutions of Dy1 and Dy2 were 1.2% and 1.6% in sigma respectively.

Figure 8 shows the count rate dependence of the amplitude of the light from the LXe scintillation chamber. The amplitude was constant for a beam intensity of 3×10^2 -2×10^4 cps. The plot for a beam intensity of 1.3×10^5 cps is not shown in Fig. 8, because the measurement was not carried out under good conditions due to the AC-coupling of the ADC (LeCroy 2249W). The closed plots indicate Dy1 and Dy2, and they show the difference of the gain. These fluctuations were less than 1%. Figure 9 shows the count rate dependence of the energy resolution. The plots of Dy1 are distributed from 1.2% to 1.4% for a wide range of beam intensity. Those of Dy2 are between 1.4% and 1.6%.

The relationship of energy outputs from Dy1 and Dy2 for the deposited energy in LXe is shown in Fig. 10. The deposited energy in LXe was estimated by subtracting the calculated energy loss at the Havar window from the measured energy by TOF. The nonlinearity of the amount of scintillation light in LXe for the incident energy is fairly smaller than those in other organic and inorganic scintillators. Such linearity in LXe was expected because the scintillation yields in LXe were almost constant in the linear energy transfer (LET) region of $100-1000$ MeV cm^2/g .[9,10]

4.3 Relation of both resolutions to the number of photons

The number of photons that arrive on a photocathode of each PMT is estimated by the solid angles calculated along the track of the ^{20}Ne beam. The intrinsic time resolution is shown in Fig. 11 as a function of the number of photons (N), which enter the window

of PMT, and a solid curve shown in the figure is fitted by a function of $(a/\sqrt{N}+b)$, where a and b are fitting parameters. The same tendency was observed for the energy resolutions of Dy1 and Dy2, and the results are shown in Fig. 12. It is obvious that the number of photons determines the intrinsic time resolution and the energy resolution. This fact suggests that both resolutions will be improved by increasing the number of incident photons.

4.4 New design of LXe scintillation chamber for RI beam experiments

In this experiment, the geometry of PMTs covered a small solid angle of 0.2% of 4π. If PMTs are mounted near the light source, the number of observed photons will increase and both the energy and time resolutions are expected to be improved.

Figure 13 shows the structural concept of a practical LXe scintillation chamber for RI beam experiments. Eight PMTs are mounted near the circumference of the beam window and four PMTs are used at the back.

Based on an estimation of solid angles, the number of photons observed by one PMT at the back will increase to sixfold. The estimation from the fitting curve in Fig. 11 shows that the intrinsic time resolution will be improved up to 20 ps.

Furthermore, the total number of photons will increase to 50-fold more than that of the chamber in this experiment. The fitting curves in Fig. 12 indicate that the energy resolution will be close to that of the noise level with an increase in the number of photons. The electric noise was only 0.2% in this experiment. Although factors other than electric noises may appear at such a high resolution, an excellent energy resolution similar to that of Si detector is expected.

5. Conclusion

The response of scintillation in LXe to heavy-ion beams was tested with an ^{20}Ne beam at an energy of 135A MeV. The intrinsic time resolution was about 30 ps in sigma at a beam intensity of up to 1.3×10^5 cps. The energy response was stable at a beam intensity of up to 2×10^4 cps, and energy resolution was 1.2% in sigma. A realistic design of a LXe scintillation chamber for use as an energy spectrometer and a timing detector for heavy-ion beams were also demonstrated. It was shown that both time and energy resolutions

will improve greatly.

Acknowledgements

The authors wish to express their thanks to the staff of the RIKEN Ring Cyclotron for their operation of the accelerator, and Dr. R. Kanungo for critical reading of the manuscript. One of the authors (T.K.) is grateful for the support from the Junior Research Associate (JRA) of RIKEN.

References

1) I. Tanihata: Nucl. Phys. A **616** (1997) 56c.

2) H. Sakurai et al.: Phys. Lett. B **448** (1999) 180.

3) A. Yunoki, T. Doke, N. Fukuda, M. Kase, T. Kato, J. Kikuchi, K. Masuda, M. Niimura, H. Okada, K. Ozaki, Y. Piao, E. Shibamura, M. Tanaka, I. Tanihata and K. Terasawa: Nucl. Instrum. & Methods A **432** (1999) 332.

4) A. Yunoki, T. Doke, M. Kase, T. Kashiwagi, T. Kato, J. Kikuchi, K. Masuda, M. Niimura, K. Ozaki, E. Shibamura, M. Tanaka and I. Tanihata: Jpn. J. Appl. Phys. **38** (1999) 6491.

5) O. Cheshnovski, B. Raz and J. Jortner: Chem. Phys. Lett. **15** (1972) 475.

6) A. Hitachi and T. Takahashi: Phys. Rev. B **27** (1983) 5279.

7) M. Miyajima and S. Sasaki: Nucl. Instrum. & Methods B **63** (1992) 297.

8) N. Ishida et al.: Nucl. Instrum. & Methods A **384** (1997) 380.

9) T. Doke, H. J. Crawford, A. Hitachi, J. Kikuchi, P. J. Lindstrom, K. Masuda, E. Shibamura and T. Takahashi: Nucl. Instrum. & Methods A **269** (1988) 291.

10) M. Tanaka, T. Doke, A. Hitachi, T. Kato, J. Kikuchi, K. Masuda, T. Murakami, F. Nishikido, H. Okada, K. Ozaki, E. Shibamura and E. Yoshihira: Nucl. Instrum. & Methods A **457** (2001) 454.

Figure captions

Fig. 1. A cross-sectional view of the LXe scintillation chamber.

Fig. 2. A cross-sectional view of the internal vessel. Two PMTs are mounted on the outer vessel, side by side. They have no contact with the internal vessel. A diode-type chamber was installed on the top in order to check the purity of LXe.

Fig. 3. The breeder circuit of PMTs for the LXe scintillation chamber. D1-D10: dynodes. HV0: high-voltage supply. HV1-HV3: boosters for current supply, P.C: photocathode. Dy1 and Dy2: signals from each dynode.

Fig. 4. A schematic drawing of the experimental setup.

Fig. 5. Typical time-difference spectrum between PMT A and PMT B for ^{20}Ne ions at an energy of 2.5 GeV.

Fig. 6. The intrinsic time resolution as a function of beam intensity.

Fig. 7. (a): Typical energy spectrum obtained from Dy1 for ^{20}Ne ions at an energy of 2.5 GeV. (b): Typical energy spectrum of Dy2 under the same condition as that in (a).

Fig. 8. The amplitude of the observed scintillation light as a function of beam intensity. ADC channels were compressed to a quarter size. (▲): sum signals of Dy1s, (•): sum signals of Dy2s.

Fig. 9. The energy resolution as a function of beam intensity. (▲): Dy1(A+B), (•): Dy2(A+B)

Fig. 10. Relationship between the amplitude of the output signals and the deposited energy in LXe. ADC channels were compressed to a quarter size. (▲): Dy1(A+B), (•): Dy2(A+B)

Fig. 11. The intrinsic time resolution as a function of the number of photons, which arrive on a photocathode of one PMT. The solid curve is fitted by $(a/\sqrt{N}+b)$, where N is the number of photons, and a and b are fitting parameters.

Fig. 12. Energy resolution as a function of the number of photons, which arrive on a photocathode of any PMTs. The solid curves are fitted by $(a/\sqrt{N}+b)$, where N is the number of photons, and a and b are fitting parameters.

Fig. 13. Schematics of the newly designed LXe scintillation chamber. In this case, 12 PMTs are used.

Fig. 1
Toshiyuki Kato

7 cm

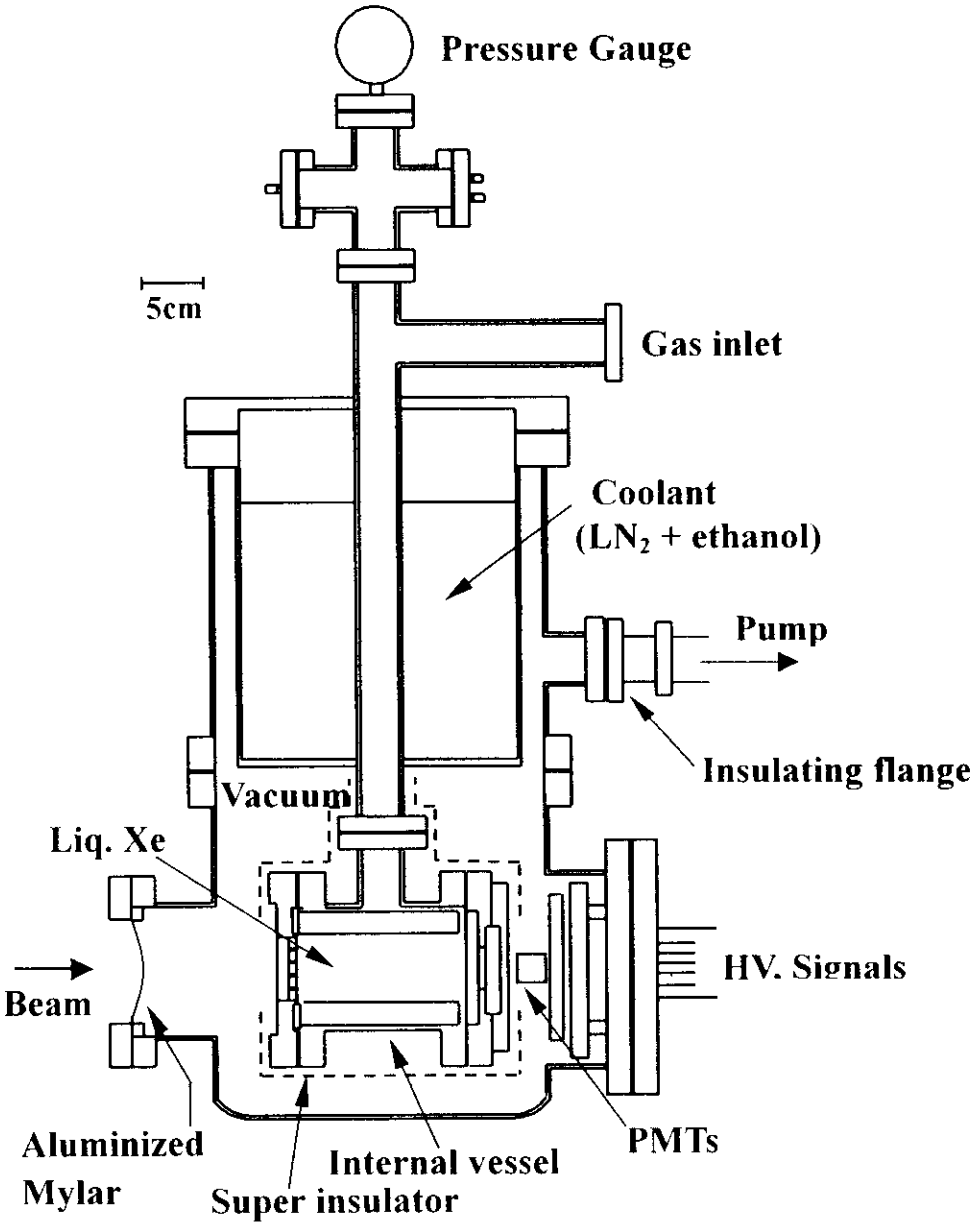

Fig. 2
Toshiyuki Kato

8.6 cm

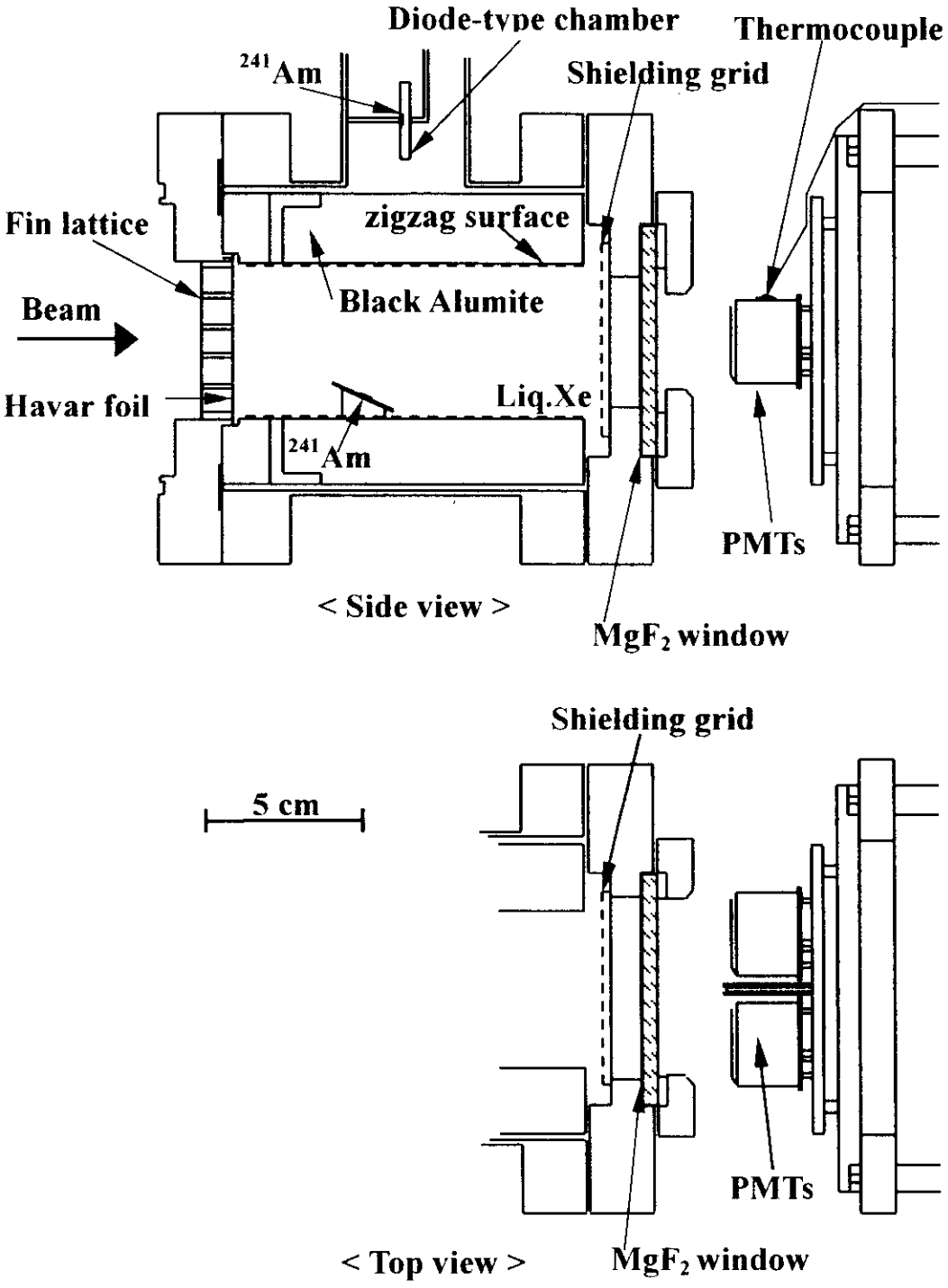

Fig. 3
Toshiyuki Kato

8.6 cm

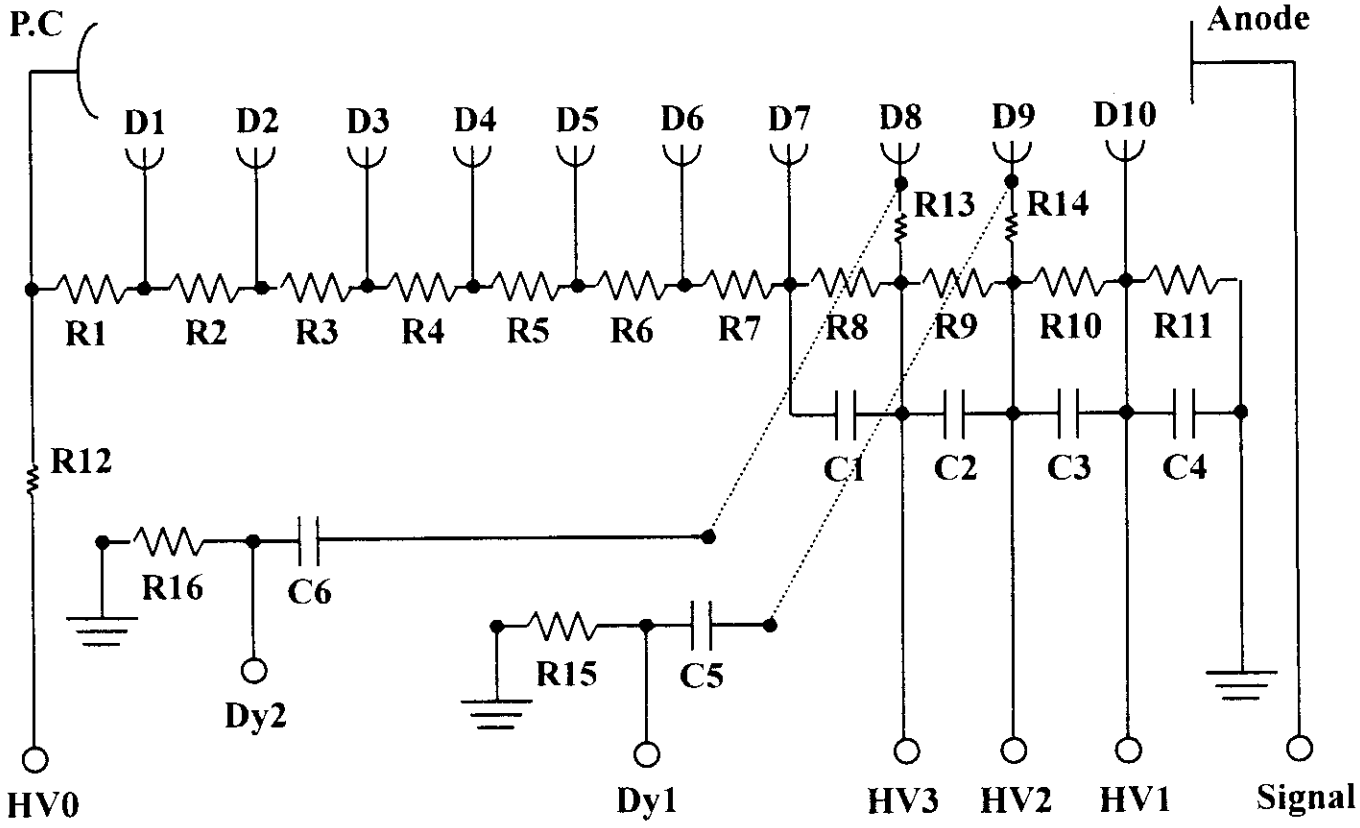

R1~R3	: 90 kΩ	C1~C4	: 0.02 μF
R4~R10	: 60 kΩ	C5~C6	: 0.01μF
R11	: 30 kΩ		
R12~R14	: 51 kΩ		
R15~R16	: 100 kΩ		

Fig. 4
Toshiyuki Kato

8.6 cm

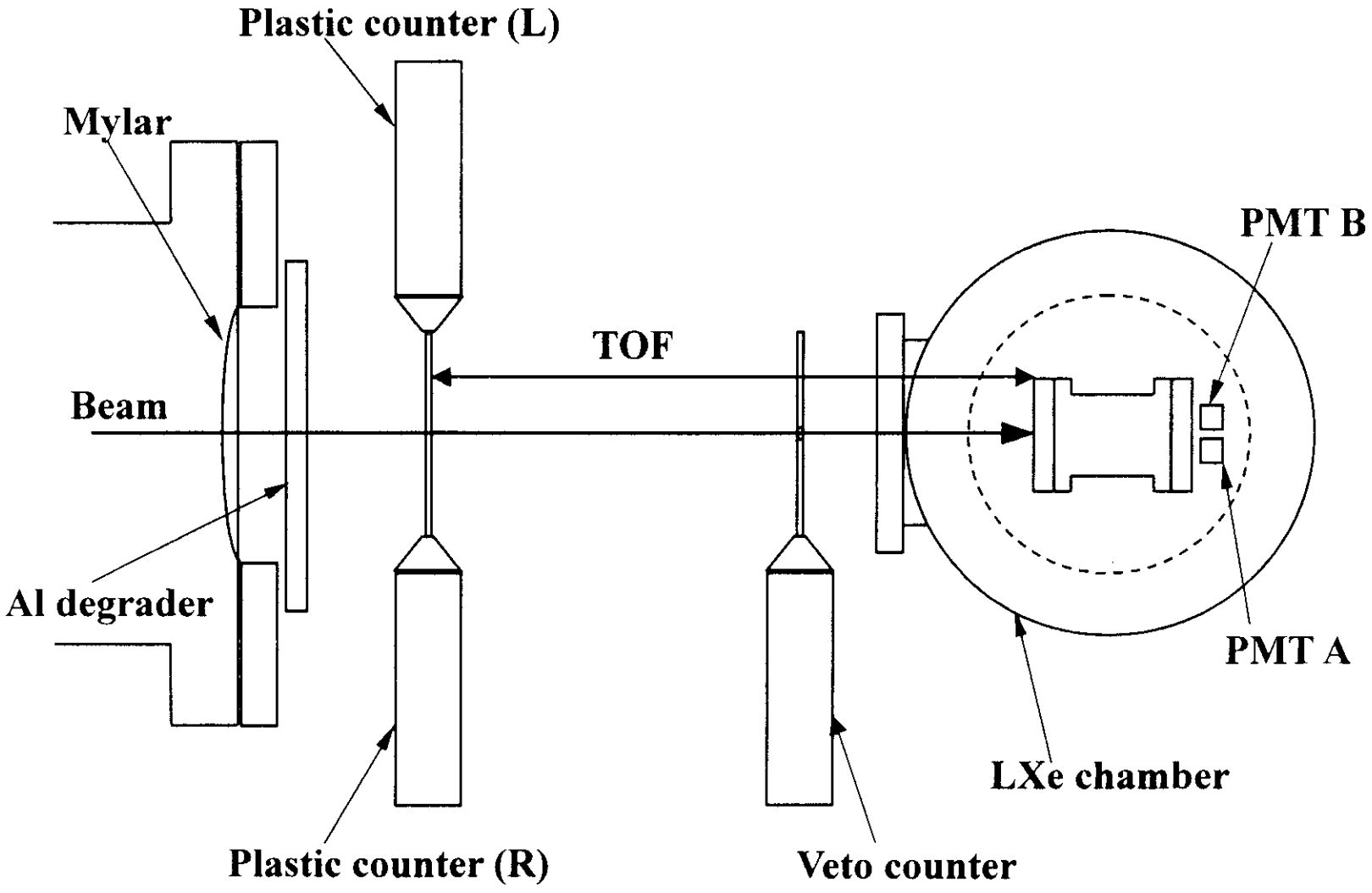

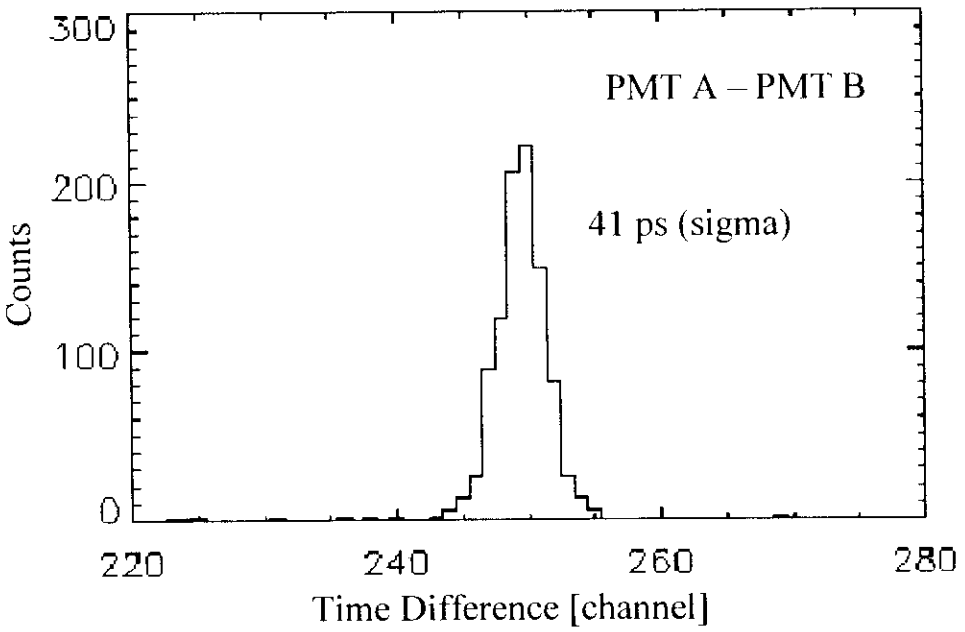

Fig. 5 Toshiyuki Kato (8.6 cm)

Fig. 6
Toshiyuki Kato

8.6 cm

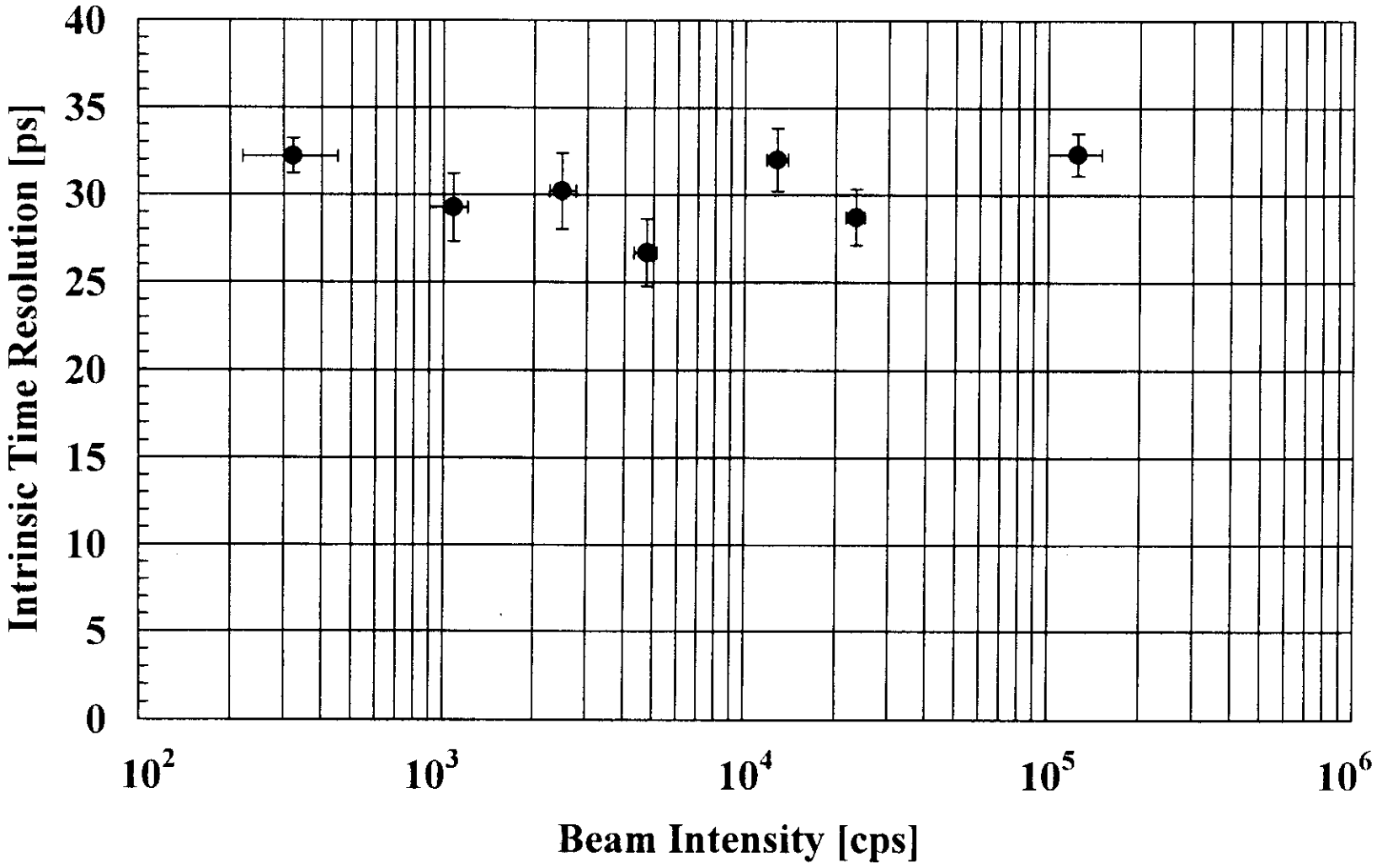

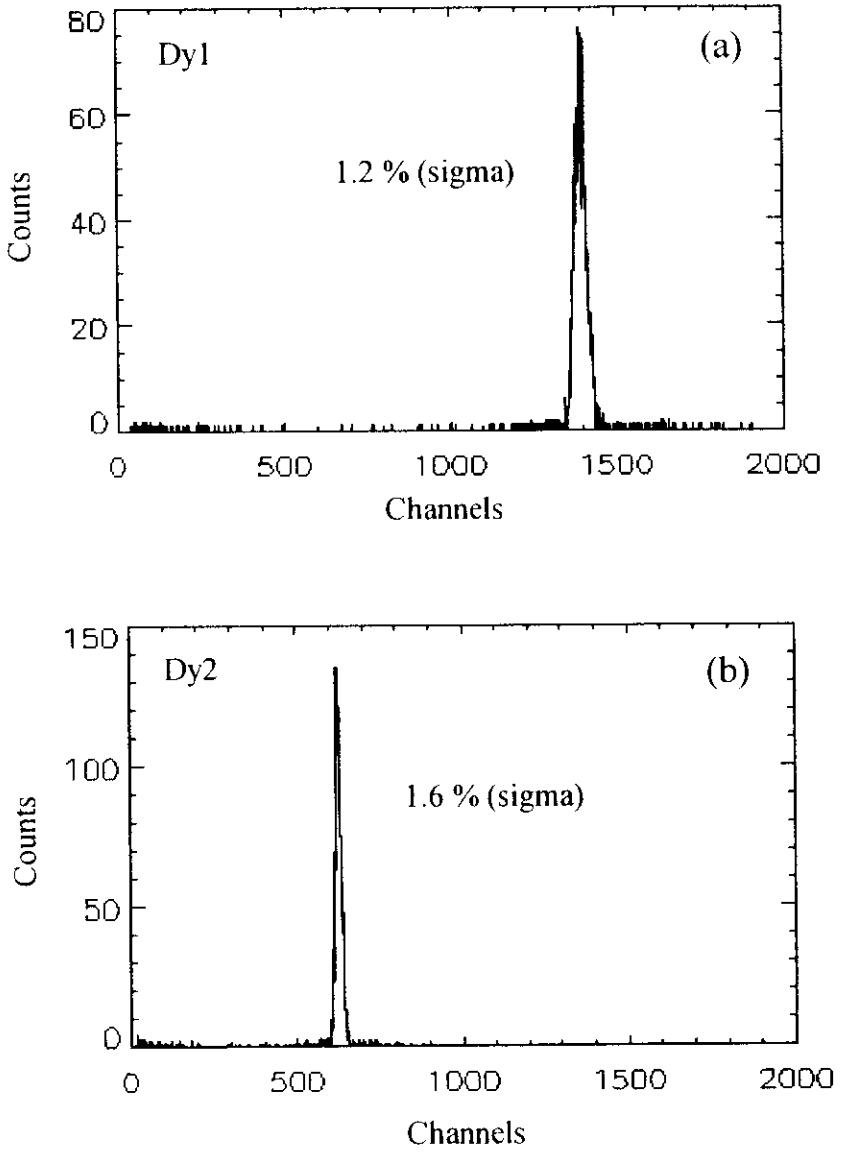

Fig. 7 (a) (b) Toshiyuki Kato (8.6 cm)

Fig. 8
Toshiyuki Kato

8.6 cm

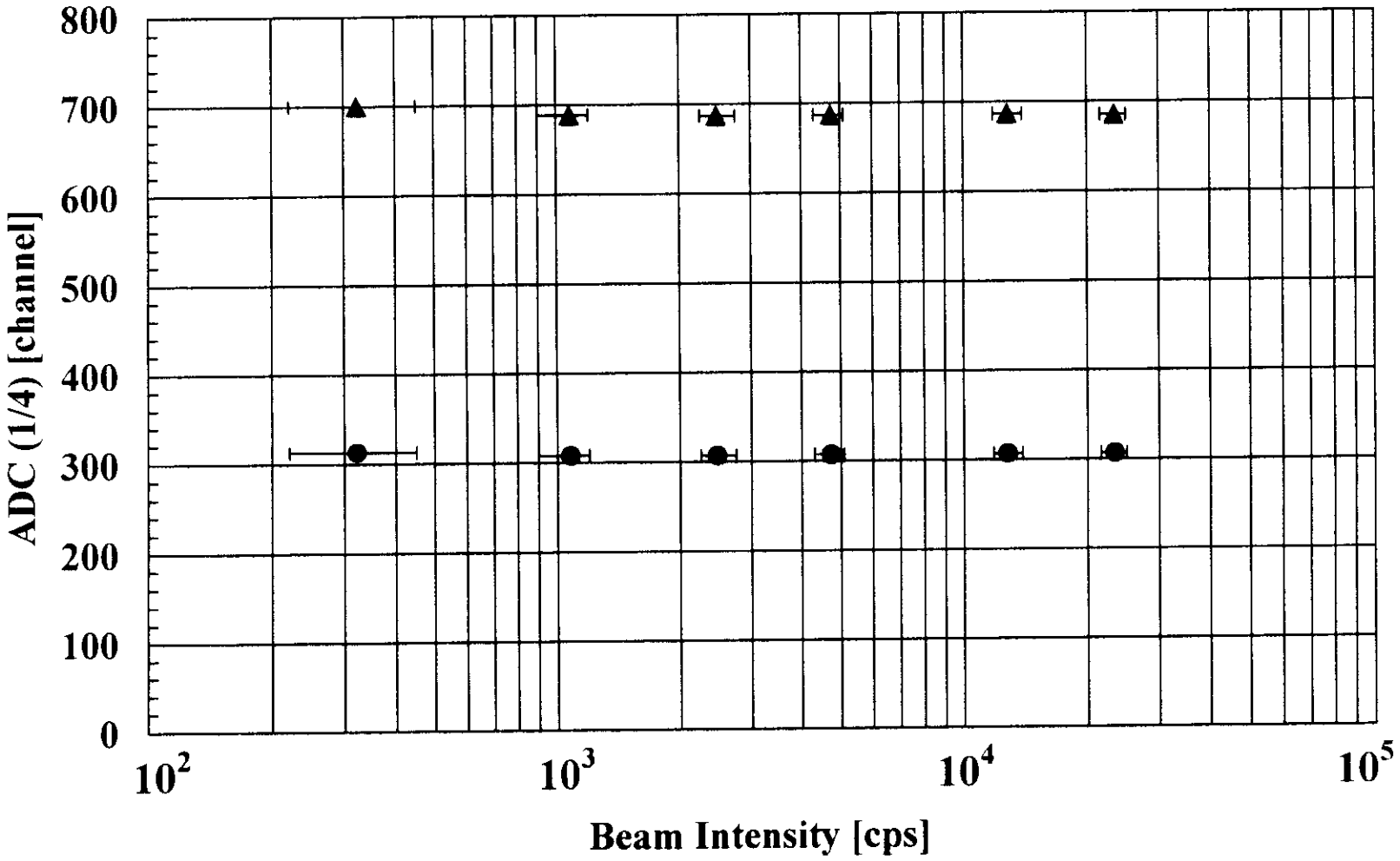

8.6 cm

Fig. 9
Toshiyuki Kato

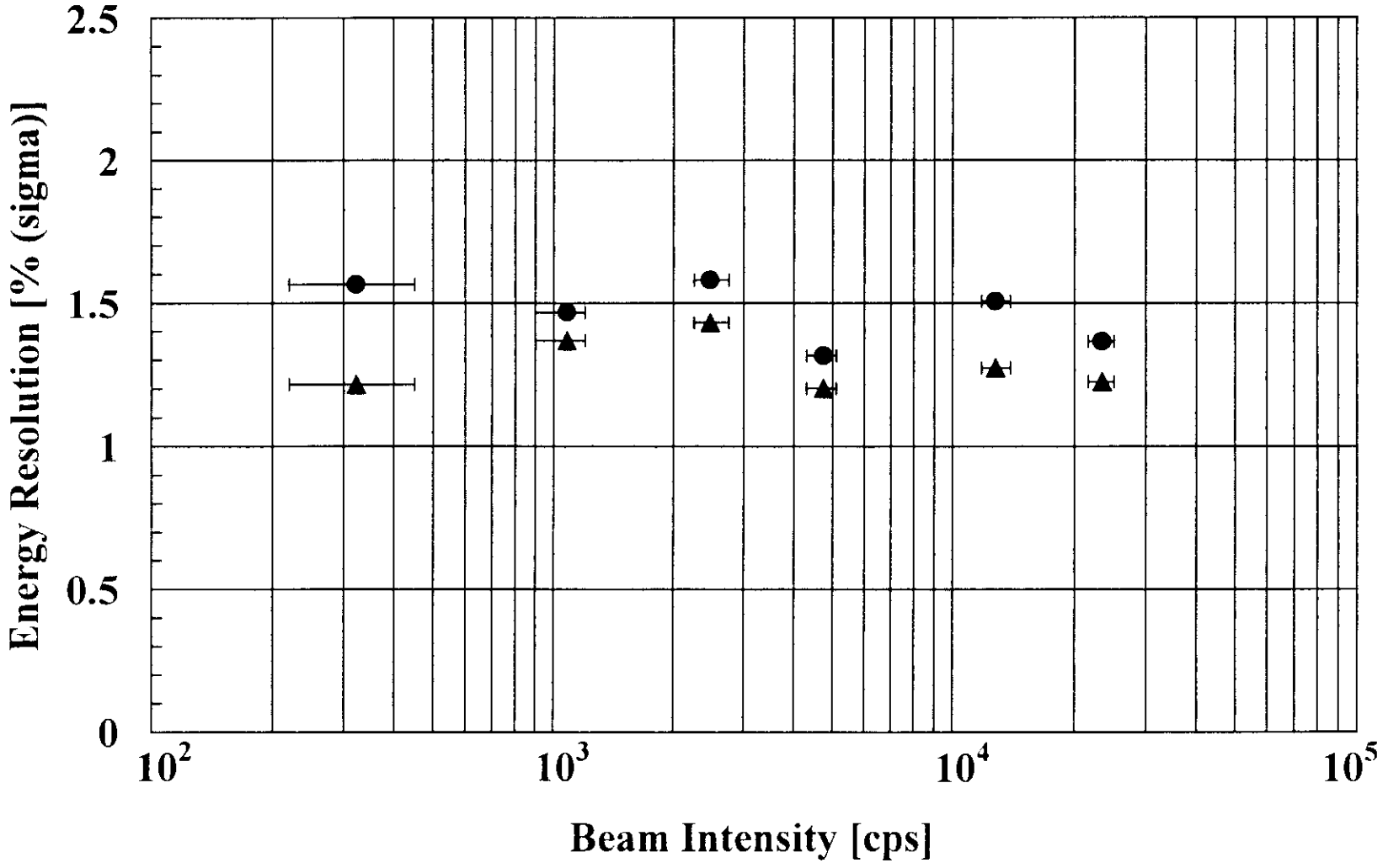

Fig. 10
Toshiyuki Kato

8.6 cm

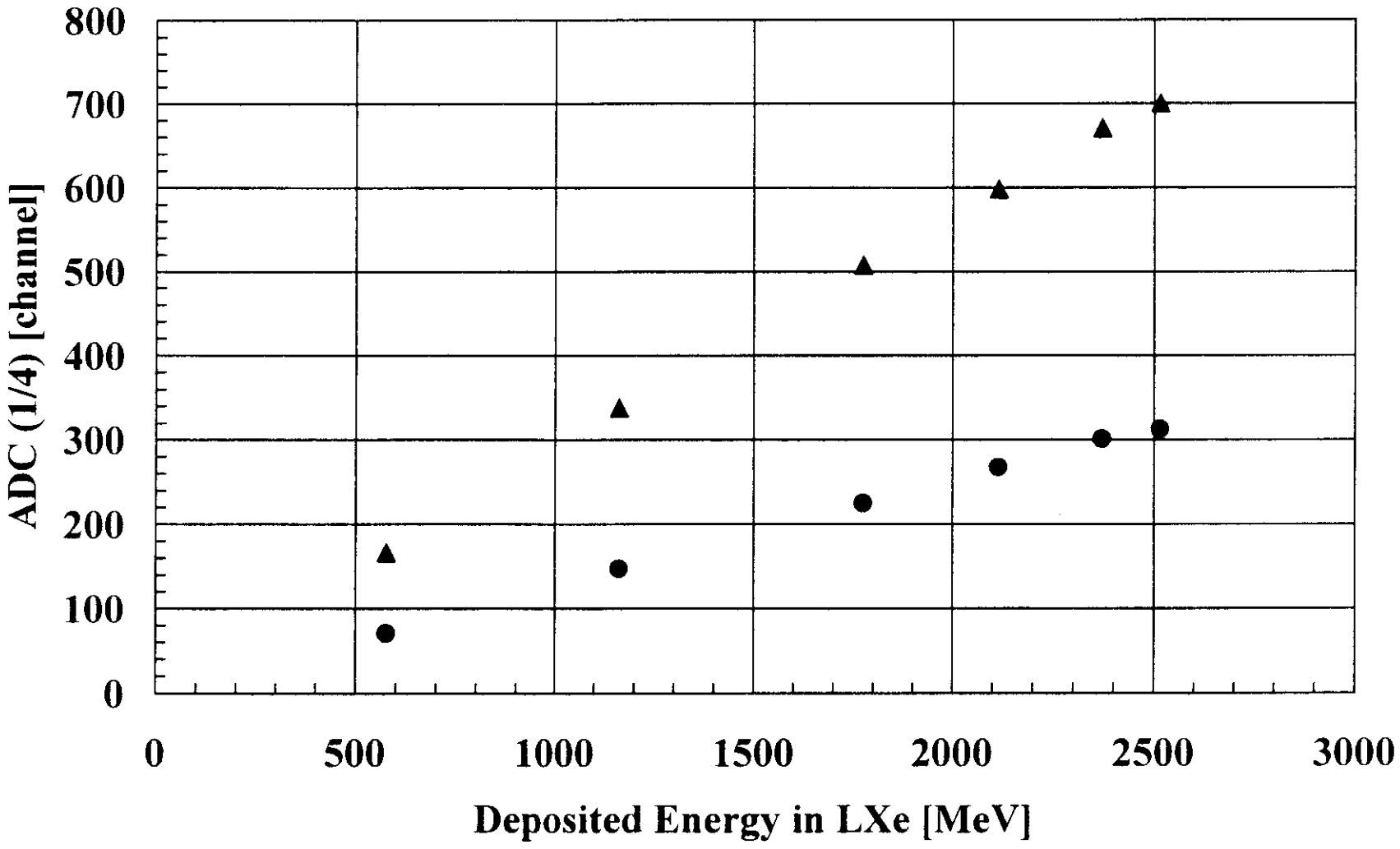

8.6 cm

Fig. 11
Toshiyuki Kato

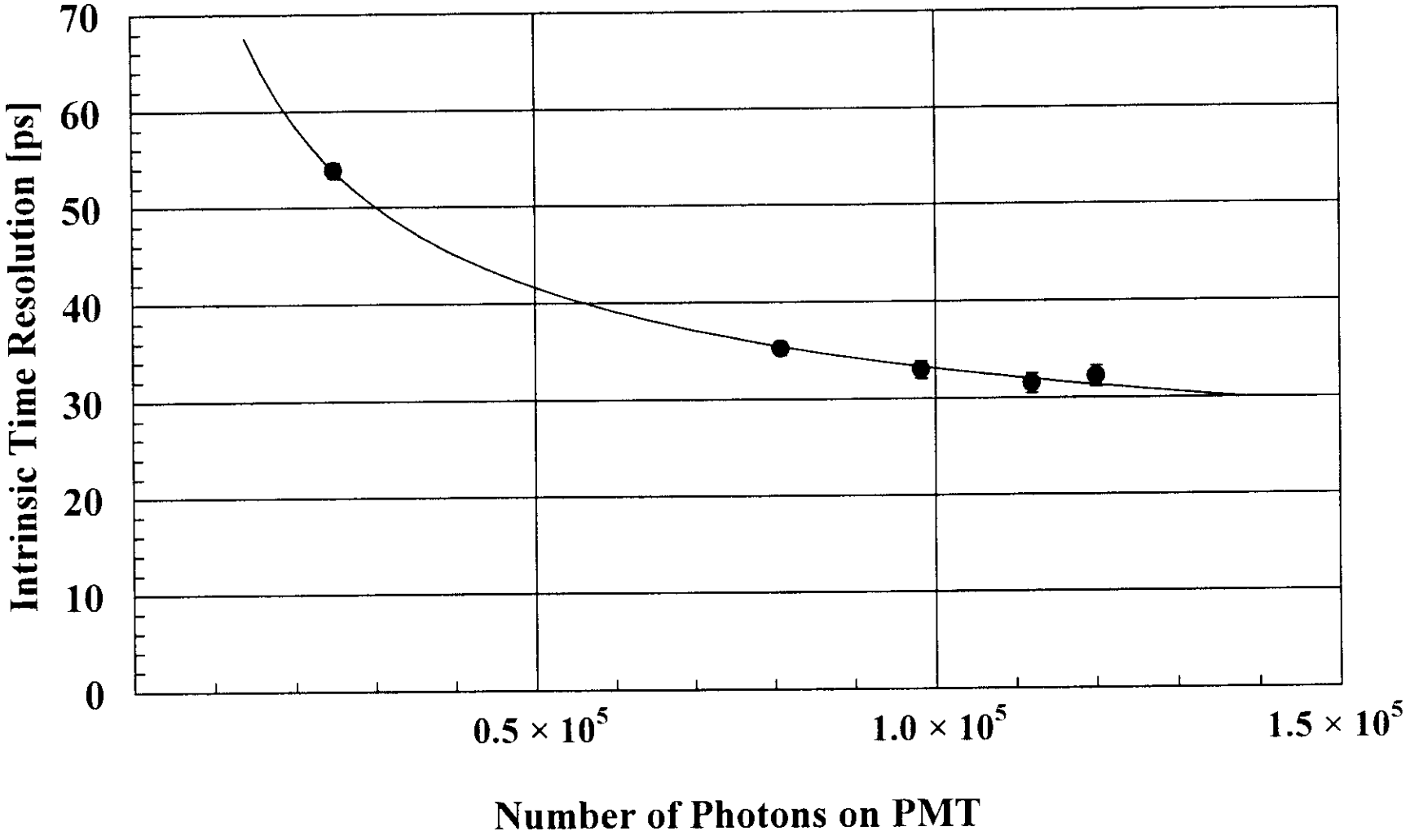

8.6 cm

Fig. 12
Toshiyuki Kato

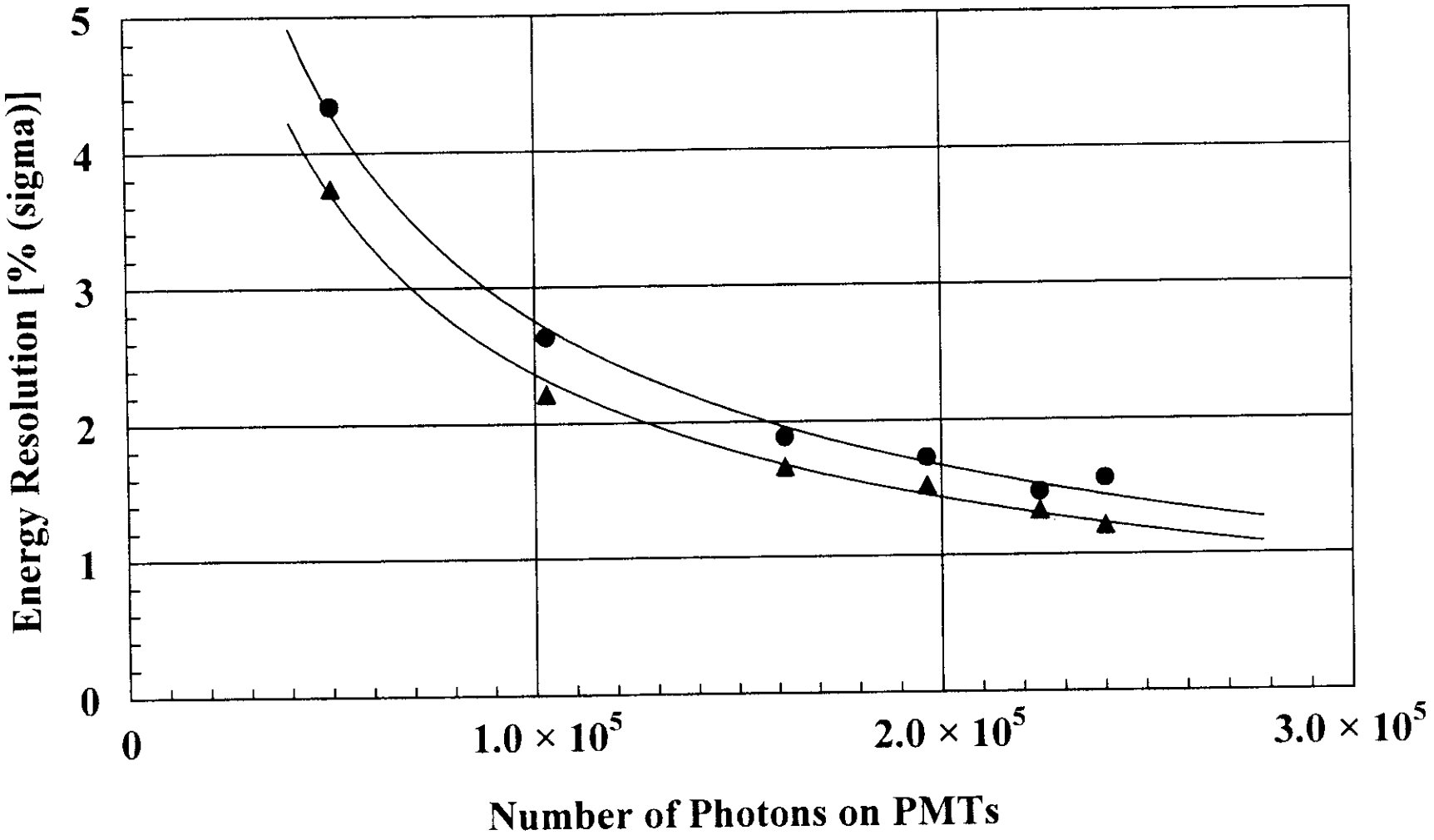

Fig. 13
Toshiyuki Kato

8.6 cm